Spring 5-2022

Solvent Effects in Phenol Hydrogenation on a Supported Ruthenium Catalyst

Daniel McKeon

SOLVENT EFFECTS IN PHENOL HYDROGENATION ON A SUPPORTED RUTHENIUM CATALYST

by

Daniel McKeon

A Thesis Submitted in Partial Fulfillment
of the Requirements for a Degree with Honors
(Chemical Engineering)

The Honors College

University of Maine

May 2022

Advisory Committee:

Thomas J. Schwartz, Associate Professor of Chemical Engineering, Advisor
François G. Amar, Professor of Chemistry
Brian G. Frederick, Associate Professor of Chemistry
G. Peter van Walsum, Professor of Chemical Engineering
M. Clayton Wheeler, Professor of Chemical Engineering

ABSTRACT

Growing concerns around climate have piqued interest in using biobased alternatives in place of fuels and chemicals traditionally made from petroleum. Lignocellulosic biomass has been noted for its potential as a biobased chemical precursor in the context of a biorefinery. It can be pyrolyzed to yield an oil, but catalytic upgrading is required to lower oxygen content to suitable levels. Ruthenium supported on titania has been identified as a catalyst suitable for hydrodeoxygenation of oxygenated aromatic pyrolysis products in the liquid phase. In liquid phase reactions, intermolecular attractions between the solvent and the reactants can significantly change chemical activities and thus reaction rates. This thesis investigates solvent effects on the hydrogenation rate of phenol over ruthenium supported on titania. Use of a model compound allows detailed kinetics studies to be performed which help gather insight into the more complex kinetics of biomass reactions. Phenol is chosen as a model compound for lignocellulosic biomass hydrodeoxygenation, as it has shown the most resistance to deoxygenation. This work investigates phenol hydrogenation in various solvents and identifies a significant solvent effect that can be attributed to differences in activity coefficients in the desorption of the first product in the hydrogenation reaction of phenol. The trend of rate effects from solvents is not obvious, with 1-butanol and isopropanol producing significantly different rates, and no trend with polarity is observed across the solvents. This warrants the use of transition state theory expressions to sufficiently analyze the phenomena observed.

ACKNOWLEDGEMENTS

I would like to thank all those who have helped me along the way, for without them this work would not have been possible. First, I would like to thank my family who has supported me through my entire journey and shown me how to create something to be proud of. I would also like to thank my friends, from my time at UMaine and before, for encouragement along the way and being willing to listen to every new problem I encountered in this work. To the members of the UMaine Catalysis Group, thank you for all of the time you spent showing me how to improve my work, and your invaluable lessons in performing research in a catalysis lab. Most importantly, thank you for welcoming me into the group; I enjoyed learning alongside you. I would like to thank my entire committee for guiding me in this process and for helping me to understand the principles behind the project. And last, I would like to thank Dr. Schwartz, for your patience and guidance throughout this process. I can't say how grateful I am. Thank you.

TABLE OF CONTENTS

LIST OF FIGURES

LIST OF TABLES

INTRODUCTION

The Demand for Biobased Chemicals and Fuels

The world population and standards for quality of life are continually growing, resulting in a high pressure to increase production of many end products currently supplied by fossil fuels. Climate change is among the leading issues the world faces in the 21st century, and the problem is exacerbated by this continual growth. Alternative routes to produce chemicals supplied traditionally by the oil and gas industry thus have an increased focus in their development. Biobased reactions from forest residues provide a suitable method to reduce lifecycle emissions and lessen cost fluctuations for transportation fuels and sectors of the commercial chemical industry.[1,2] While other solutions such as solar and wind farms can provide clean power in the form of electricity, biobased production provides a practical solution for the transportation industry, as additives and blendstocks could be produced as 'drop-in' fuels that would be compatible with existing technology. Further, many modern materials require chemicals derived from petroleum products; again, biobased chemical production is uniquely suited to provide an alternative solution and is perhaps one of the only practical solutions.

A recent study[1] has shown that under various climate effect mitigation scenarios, biomass provides up to 35% of total energy by 2050; a baseline scenario from the model shows that biomass would supply 8% of total energy by 2050. Similarly, the biochemical industry is projected to grow, with a compound annual growth rate of 12.6% from 2018 – 2025 (calculated in 2019).[3] Lignocellulosic feedstocks have great potential for use due to their higher yields as compared to other energy crops; higher yields drive down land use. Land use is tied to bio-based chemical and fuel production rates and limits the

environmental benefits from new grassroots production. A long-standing discussion of 'food vs fuel' raises the point that land used for food crop production should not be used for energy crop production. A study[3] published in 2020 utilized an integrated global computable general equilibrium model and showed that if land use grows too quickly, the environmental benefits may be reversed. This could be a realizable effect; the model assumes a 1.5% annual decrease in biomass conversion costs, which leads to growth in the biochemical sector. The increased demand for bioproducts leads to an increased demand for biomass – which means energy crops must be utilized in addition to waste streams. This puts pressure on the agricultural industry and leads to the deforestation of unmanaged lands. This deforestation is depicted globally in Figure 1.

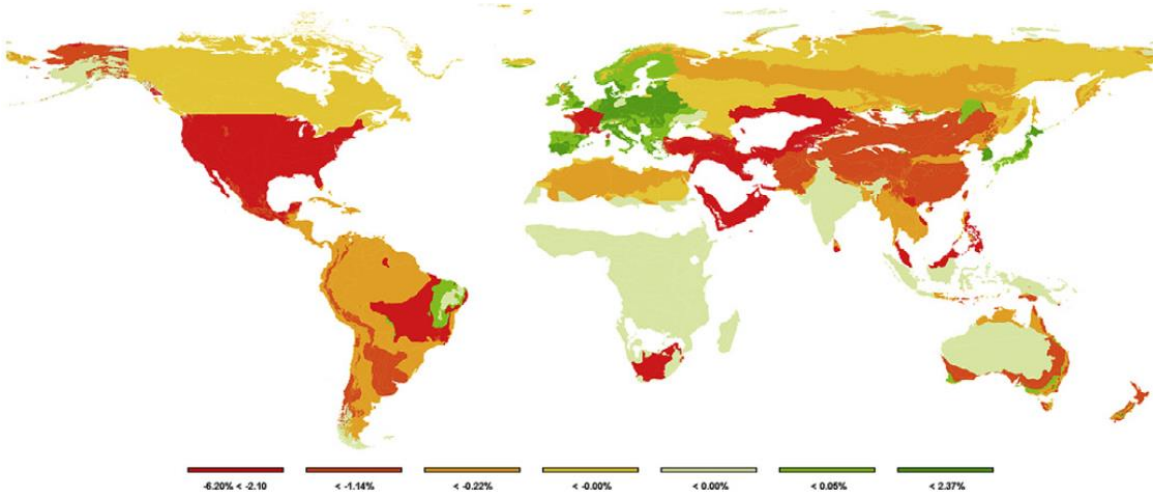

Figure 1. Unmanaged and/or natural forest change in 2050 as compared to a 2011 baseline. Adapted from Nong et. al.

These land usage change (LUC) effects outweigh the reduced CO_2eq. (the mass of carbon dioxide emissions with a global-warming potential of the gas referenced[4]) emissions from reduced fossil fuel use, resulting in a net increase in emissions at 2050. This emphasizes the importance of bioproduct pathways from forest waste residues, one of which is lignin.

Lignin-containing forest waste residues can be produced as byproducts from the lumber and pulp and paper industries. Many companies in these industries adhere to standards that show they are managing their forest lands.[5] This reduces emissions without the effects of deforestation.

Pyrolysis

There are a variety of paths from crude biomass to useful chemicals. Some prominent options include gasification, biological processes that use enzymes, and pyrolysis. Pyrolysis offers some advantages in that it has been found to be more economical compared to other methods.[6] Pyrolysis consists of heating biomass to high temperatures (~500 °C) in the absence of oxygen. This depolymerizes the biomass into a range of small organic compounds, which can be further upgraded to useful chemicals. There are two primary methods of pyrolysis: fast pyrolysis and slow pyrolysis. The different residence times affect the selectivity of the reaction, with bio-oil being the primary product of fast pyrolysis and biochar being the primary product of slow pyrolysis. Fast pyrolysis has garnered attention due to its selectivity for oil. As discussed earlier, bio-oil has a significant role to play in mitigating fossil fuel use due to its ability to act as a drop-in fuel or additive, and also be used in situations where electricity is not a viable power source, such as the airline industry. Figure 2 below shows a compilation of pyrolysis yields from many different reactor setups and feedstock compositions.[7] Feedstock and operating conditions including temperature, moisture, and residence time impact liquid oil yield, and at optimal conditions, fast pyrolysis can have yields upwards of 70 wt%.

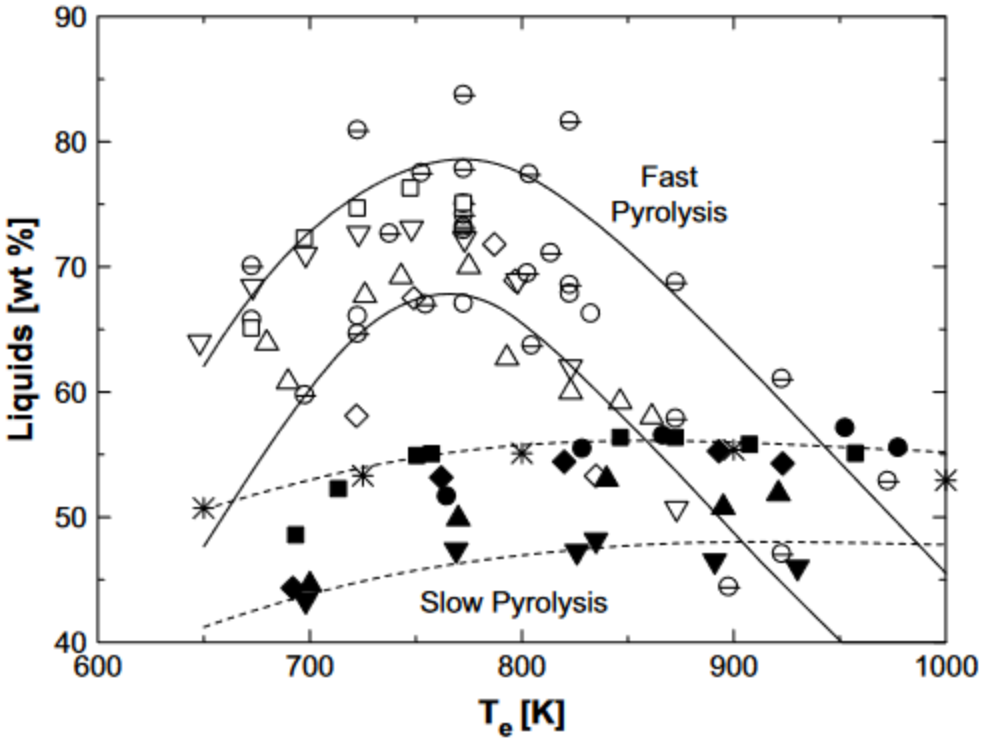

*Figure 2. Liquid yields (on dry solid % basis) for pyrolysis in fluidized bed reactors at different heating temperatures. Hardwood species shown by ϴ, ∇, ∆; softwood species shown by ○, ◊, □; * shows fixed-bed pyrolysis of beech wood. Pyrolysis of 40mm diameter cylinders of hardwood indicated by ■, ∇; pyrolysis of 40mm diameter cylinders of softwood indicated by ●, ▲, ◆. Adapted from Di Blasi et. al.*

Pyrolysis oil itself is not typically sold as a fuel alternative, as most applications are not tolerant of its composition of aromatic products with a high oxygen content. This gives the oil undesirable traits such as high acidity, corrosiveness, high viscosity, high reactivity and lower heating values.[8] The bio-oil can be upgraded through catalysis, leading to stable molecules with more desirable physical properties.

Catalytic Hydrodeoxygenation

A primary part of this upgrading is deoxygenation. Phenolic compounds are prevalent in the pyrolysis product mixture,[9] and these compounds provide more value with the oxygen removed, as the high oxygen content is one of the major attributes that gives the oil a low

heating value[8]. Catalytic hydrodeoxygenation offers a promising and necessary route for upgrading oxygenated aromatic compounds. Catalytic hydrodeoxygenation is the process of removing oxygen from hydrocarbon molecules through specially designed metal and metal oxide heterogeneous catalysts.

Hydrotreating of carbonaceous material is conventional in petroleum reforming, where hydrodesulfurization (HDS) and hydrodenitrogenation (HDN) are more common than hydrodeoxygenation (HDO) due to the significant sulfur and nitrogen of oil. In bio-oils, nitrogen and sulfur content are negligible, while the oxygen content accounts for 35 – 40 wt% of the mixture.[8] Catalyst design for the upgrading of bio-oils has been the subject of much research in recent years, as heterogeneous catalysis has potential to very selectively upgrade pyrolysis oil to valuable products.

Solvent Effects

Several factors are important in hydrodeoxygenation reactions. A topic of interest is the solvent used for the reaction. A solvent is a critical piece for the condensed phase reaction and can not only act as a reaction medium but also change the rate of the reaction in several ways. The nature of the solvent can impact the solvation of the adsorbed reactants, products, or transition states, as well as influencing diffusion of the reactants and the products from the surface to the bulk fluid.

Transition state theory provides a rigorous framework in which to examine solvent effects, and has been used to analytically determine the extent to which a solvent has an effect on a reaction rate.[10,11]

Equation 1 shows the general form of a rate equation from transition state theory.

$$r = \frac{k_B T}{h} \frac{K^{\ddagger}}{\gamma^{\ddagger}} a_A a_B \quad (1)$$

Madon and Iglesia describe an example where solvent effects play a key role in evaluating a reaction mechanism.[11] The hydrogenation of cyclohexene occurs according to different mechanisms when on Pt and Pd catalysts. On a Pt catalyst, the reaction rate of cyclohexene hydrogenation is dependent on the concentration of hydrogen in the solvent. Thus, the solvation ability of the liquid solvent chosen affects the rate of reaction.

$$r_{Pt} = k_{O\_Pt} C_{H_{2(l)}} \quad (2)$$

When the catalyst is Pd, the identity of the solvent does not affect the rate of reaction; instead, the rate scales with the square root of the partial pressure of hydrogen in the vapor phase.

$$r_{Pd} = k_{O\_Pd} \sqrt{P_{H_{2(g)}}} \quad (3)$$

Madon and Iglesia show that these results and the differences in the rates between the catalysts can be described with transition state theory.

When the reaction occurs on a Pt catalyst, the rate determining step is the dissociative adsorption of H_2 on the surface. The mechanism was determined to occur according to the elementary steps below.[12]

1. Hydrogen gas absorption $H_2(g) \leftrightarrow H_2(l)$
2. Hydrogen gas physisorption to surface $H_2(l) \leftrightarrow H_2(a)$
3. (rds) Hydrogen gas dissociation on surface $H_2(a) + ** \rightarrow 2H*$
4. Cyclohexene adsorption to surface $R + ** \rightarrow *R*$
5. Incomplete hydrogenation $*R* + H* \leftrightarrow RH* + **$

6. Complete hydrogenation and desorption $RH* + H* \rightarrow RH_2 + **$

Equating overall rate to the rate of step 3, the following equations describe the reaction. The equation takes the form from transition state theory, and is derived in more detail in the original source.[11]

$$r_3 = \frac{k_B T}{h} \frac{K^{\ddagger}}{\gamma^{\ddagger}} a_{H_2(a)} a_{**} \tag{4}$$

Equation 4 can be simplified.

$$r_{Pt} = k' \frac{N}{V} \frac{1}{\gamma^{\ddagger}} a_{H_2(l)} = k' \frac{N}{V} \frac{\gamma_{H_2(l)}}{\gamma^{\ddagger}} x_{H_2(l)} \tag{5}$$

The structure of adsorbed hydrogen is similar to the transition state structure, which leads to similar activity coefficients, and thus the ratio is approximately unity. This leads to the apparent rate being dependent on concentration even though the true driving force is activity.

The following elementary steps describe the catalytic cycle of cyclohexene hydrogenation on Pd.[13]

1. Hydrogen gas absorption $H_2(g) \leftrightarrow H_2(l)$
2. Hydrogen gas physisorption to surface $H_2(l) \leftrightarrow H_2(a)$
3. Hydrogen gas dissociation on surface $H_2(a) + ** \leftrightarrow 2H*$
4. Cyclohexene adsorption to surface $R + ** \leftrightarrow *R*$
5. Incomplete hydrogenation $*R* + H* \leftrightarrow RH* + **$
6. (rds) Complete hydrogenation and desorption $RH* + H* \rightarrow RH_2 + **$

Equating the rate of step 6 to the overall rate, as was done with platinum, gives the following equation.

$$r_6 = \frac{k_B T}{h} \frac{K^{\ddagger}}{\gamma^{\ddagger}} a_{RH*} a_{H*} \tag{6}$$

Madon and Iglesia show how the expression can be simplified to match the apparent rate. Their final result is displayed below in equation 7.

$$r_{Pd} = k\frac{\gamma_{RH*}}{\gamma^{\ddagger}}\sqrt{C_{H_2(g)}} \quad (7)$$

The species RH* is adsorbed to the palladium surface, and thus unaffected by a change in solvent identity. As this ratio is independent of solvent, the reaction proceeds according to activity of the gas phase hydrogen. The activity coefficient of the gas phase hydrogen can be assumed to be unity, leading to the observed dependence of gas phase hydrogen concentration, and thus hydrogen pressure.

Similar solvent effects can be observed in hydrogenation reactions of other unsaturated compounds.[14,15] The goal of this research is to identify solvent effects in the hydrogenation of phenol on a titania supported ruthenium catalyst.

Past Work in the Hydrodeoxygenation of Phenol

The reduction of phenol in heterogeneous catalysis has been investigated due to its prominence as a model compound for lignin, a candidate for biomass refining. Lignin is a complicated polymer primarily made from phenylpropane units with a high degree of cross linking primarily from ether bonds.[16] Hydrodeoxygenation of pyrolysis bio-oil is a reaction of interest for biomass upgrading, but its complicated kinetics can be better understood through the use of model compounds, where reaction kinetics can be solved more precisely. Phenol is used as a model compound as the removal of the last oxygen on an aromatic ring has been shown to have the highest energy barriers.[17,18]

On a ruthenium catalyst with a titania support in a reducing environment, phenol has two primary reactions. Hydrogenolysis, which occurs via the direct deoxygenation pathway (DDO) and hydrogenation, which occurs by hydrogenating the aromatic ring and

dehydrating a subsequent cyclohexanol (HYD). The DDO pathway involves cleavage of a C-O bond, forming a water molecule and a benzene molecule, and has been observed to occur at interfacial sites on Ru/TiO_2 catalysts.[19]

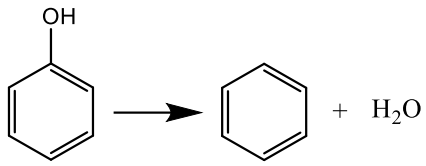

Figure 3. Phenol direct deoxygenation reaction pathway.

Previous experiments[19–22] on this reaction have focused on the more hydrogen efficient DDO route to yield benzene. The catalyst Ru/TiO_2 has been of interest due to its high selectivity for the DDO pathway over the HYD pathway. In 2015, Nelson et. al.[19] proposed a mechanism using DFT and isotopic experiments that would explain both the high selectivity and an observed effect with water as a co-catalyst.

Abdulazeez[21] investigated the reaction in a flow reactor, comparing results to those from reactions in a batch reactor, and used the solvent tetrahydrofuran to enhance the activity of phenol in the liquid phase. Deactivation of the catalyst was observed in trials run in a solvent.

Stück[20] later used decalin as a solvent and calculated smaller deactivation constants. The kinetic analysis performed showed an intricate reliance of reaction order on TiO_2 phase as well as water concentration. It was determined there were multiple competing mechanisms and changing the regime of the reaction would cause certain mechanisms to be favored, leading to different reaction orders under different conditions.

Phenol Hydrogenation

Most of the past work was focused on the hydrogen efficient DDO reaction pathway. However, saturation of the aromatic ring is important for the production of diesel

blendstocks and is a part of other biobased routes to diesel additives.[23] Its mechanism has also been the subject of much research,[24,25] with phenol and other model compounds like guaiacol. Guaiacol hydrogenation has been investigated on a variety of catalysts, with a maximum yield of 95.5%.[26] Another catalyst investigated was Ru/TiO_2, which was found to have great efficiency in part due to hydrogen spillover in the liquid phase.[27] The study predicts a similar hydrogen spillover mechanism could apply to other biomass upgrading reactions. In a DFT analysis of the hydrogenation of phenol on Pt and Ni surfaces,[25] it was found that the presence of an aqueous phase and the difference between the reaction occurring in the liquid or gas phase significantly impact the energies of adsorption and thus the reaction. It is clear in hydrogenation reactions like these, effects of solvent and reaction media become important, changing how the reaction occurs.

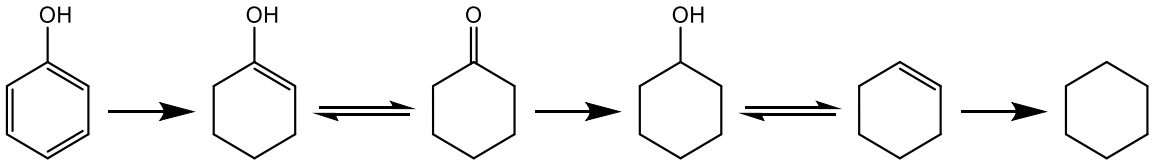

Figure 4. Phenol hydrogenation reaction pathway.

The reaction scheme of phenol hydrogenation is of interest to us, and had been identified previously.[19,28,29] Through this pathway, phenol is hydrogenated to cyclohexanol, which quickly tautomerizes to cyclohexanone. Cyclohexanone undergoes a subsequent hydrogenation, followed by a dehydration and another hydrogenation to yield cyclohexane as a final product.

The tautomerization between cyclohexenol and cyclohexanone occurs very quickly; nearly all cyclohexenol in solution will exist as cyclohexanone. Another note about the product distribution is that the hydrogenation of cyclohexene occurs very quickly, so that

if any concentration is observed, it will be very small. This has been observed in past results.[21]

Objective

Focusing on the hydrogenation pathway, the goal of this thesis is to investigate potential solvent effects in the hydrogenation of phenol. The choice of solvent in the reduction of phenolic compounds could enhance selectivity for the desired reaction pathway, DDO or HYD. The reduction of phenol over Ru/TiO_2 was carried out in a batch reactor with various solvents, and initial hydrogenation rates were calculated for the reaction in each solvent. Comparison of rates in the context of transition state theory is used to establish the presence of a solvent effect.

CHAPTER II: MATERIALS AND METHODS

Chemical Source Information

All chemicals were used as purchased, and information about all chemicals used in trials can be found below. Phenol was purchased as unstabilized loose crystals. All other reagents were purchased as liquid reagents, except for water which was produced in a MilliQ unit at 18 MΩ resistance.

Table 1. Chemical Source Information

Chemical	CAS Number	Company	Purity (wt%) and Quality notes
Phenol	108-95-2	Acros Organics	99.5
Ethyl Acetate	141-78-6	Fisher Chemical	99.9
Guaiacol	90-05-1	Acros Organics	99
Butanol	71-36-3	Fisher Chemical	99.9
Isopropanol	67-63-0	Fisher Bioreagents	99.9
Decalin	91-17-8	Alfa Aesar	cis+trans, 98
Cyclohexanone	108-94-1	Sigma-Aldrich	99.8
Cyclohexanol	108-93-0	Fisher Chemical	Reagent grade
Cyclohexane	110-82-7	Fisher Scientific	99.99
Sodium Sulfate	7757-82-6	EM Science	Anhydrous, Granular, 99.0
Hydrogen	1333-74-0	Airgas	Cylinder
Argon	7440-37-1	Matheson	Cylinder
Helium	7440-59-7	Matheson	Cylinder

Catalyst Preparation

The catalyst used was prepared for a previous project in the group and is described by Tavana.[30] In short, the catalyst was prepared using the incipient wetness impregnation method. Aqueous $Ru(NO)(NO_3)_2$ was added to the TiO_2 (P-25 from Evonik) until the

incipient wetness point was reached. The catalyst was calcined in air at 450 °C for 4 hours and reduced in Ar and subsequently H_2 at 400 °C in a quartz flow reactor for 4 hours. The catalyst was synthesized at a loading of 5wt% Ru.

The catalyst was crushed with a mortar and pestle and diluted with P-25 TiO_2 to 1wt%. Catalyst was stored in a dessicator prior to use, and it was reduced *in situ* in the batch reactor.

Reaction Trial Plan

All hydrogenation reactions were run in a 50 mL batch reactor from Parr Instrument Company. Catalyst mass and reactant mixture mass were recorded on an Ohaus pioneer bench-scale balance before each trial. Trials were run until 2 – 4 data points were collected at low conversion, less than 20% (excepting one point run in ethyl acetate at 22% conversion). Trials were run at 200 °C for 4 hours, with a 2 hour ramp time to reach temperature. After the 4 hours at 200 °C, the reactor was allowed to cool while still in the aluminum heating device, and once ambient temperature was reached, products were collected. Figure 5 shows the approximate temperature of the reactor over the duration of the trial.

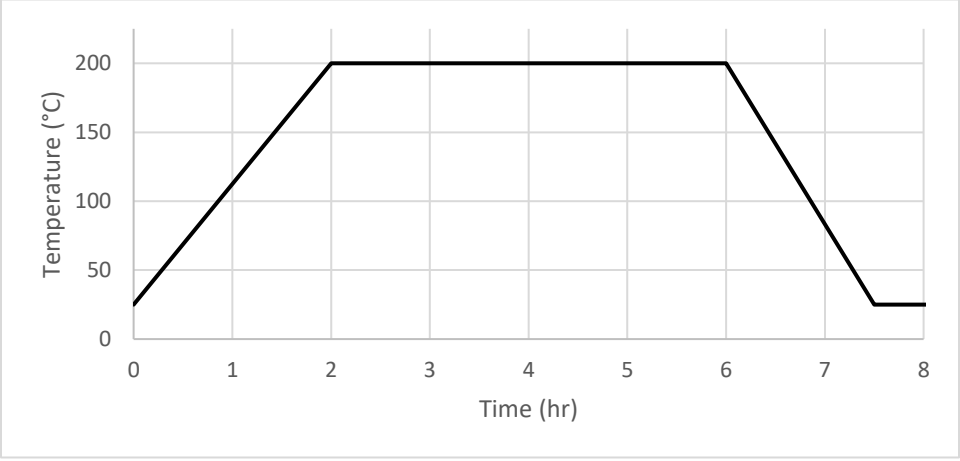

Figure 5. Temperature profile of reaction mixture over reaction time. Time to cool to ambient conditions from hour 6 is approximate.

Hydrogenation Procedure

Feed mixture was prepared at a calculated concentration of 0.53 M by measuring mass of crystallized phenol and liquid solvent on an Ohaus adventurer or Ohaus explorer bench-scale balance. Actual feed concentrations were measured using a gas chromatograph equipped with a flame ionization detector (GC-FID). Catalyst mass was adjusted between trials so that a phenol conversion of 20% or less could be obtained with 4 hours of time at 200 °C.

Massed reaction mixture and catalyst was added to the reactor with a magnetic stir bar. The reactor was then bolted shut and the vessel was placed in an aluminum tube, which acted as a furnace to evenly distribute heat to the reactor from the heating tape. The reactor headspace was then triple purged with argon and subsequently triple purged with hydrogen. After that, the reactor was pressurized with hydrogen to ~33 bar, and a magnetic plate the reactor rested on was activated to begin the stirring process.

The reactor was heated using heating tape, controlled by a PID loop through an Automation Direct SOLO 4848 temperature controller. A K-type thermocouple from Omega measured the mixture temperature, inserted into the middle of the reactor, in the liquid. There was also a temperature control loop for an emergency disabling function. A K-type thermocouple placed on the heating tape measured temperature for an Automation Direct SOLO 4824 temperature controller, to ensure the aluminum furnace did not melt. Over two hours, the temperature was brought from ambient conditions to 200 °C. Two hours was chosen as the temperature ramp time, as the heating system could not reach 200 °C in a 1.5 hour temperature ramp time. The temperature was then held at 200 °C for 4 hours, and this time is used as the reaction time in rate calculations. After the reactor

had cooled to room temperature while still inside the heating device, samples were removed, filtered with a 0.1 μm Wattman filter from the mixture containing solid catalyst particles, and inputted into the GC-FID.

Product Analysis

An Agilent Technologies GC-FID model 7820A with a 30 m DB-WAX column was used to analyze product composition quantitatively. The inlet was held at 260 °C and 16 psi, and a split ratio of 20:1 was used. The method used had an initial temperature of 40 °C which was held for 2 minutes, after which the temperature was increased to 200 °C at 10 °C/min, where it was held at for 3 minutes; so, the total time was 21 minutes. A 1.0 μL injection volume was used. The carrier gas used was He. The flame ionization detector was held at 300 °C. Standards were made in tetrahydrofuran (for phenol) and ethyl acetate (all other chemicals) for the creation of a calibration curve to translate integrated raw signal values to concentrations. These calibration curves were used for all solvents except water.

The significant difference in molecular weight between water and other organic solvents necessitates a different calibration curve. The GC-FID signal output for an integrated peak is a multiple of the number of moles of a particular chemical. For accurate mole fractions and concentrations to be calculated between different solvents with one set of calibration curves, the solvent molecular weight must be similar. The organic solvents used here have similar molecular weights, so one set of calibration curves can be used. The difference in molecular weight between water and organic solvents is large enough to require different calibration curves for samples with water as a solvent.

Thus, for trials ran in water, a different analysis method was needed. Calibration curves could be created from standards made in water, but at certain concentrations, the organic chemicals of interest separate from the aqueous phase. Cyclohexane would separate at very low concentrations. To circumvent this issue, a liquid-liquid extraction analysis method was chosen, so that if small concentrations of cyclohexane were produced, they could be detected.

Calibration curves for all chemicals are included in Appendix A.

Aqueous Solvent Product Analysis Procedure

To ensure all chemicals stayed in one liquid phase and would be present in GC injection volume in bulk concentrations, it was decided to extract products into an organic phase. Ethyl acetate was chosen as this organic phase.

When a liquid-liquid extraction is done, species in one phase transport into the other until an equilibrium is reached, with a certain composition of species in both phases. Therefore, some of the products made would remain in the aqueous phase after extraction, and an estimate of the distribution coefficient, or the ratio of concentration in the organic phase to concentration in the aqueous phase, was necessary for accurate concentrations to be obtained.

The calculation of a distribution coefficient can be avoided through use of an internal standard. A known concentration of the internal standard is added to the sample mixture. It is assumed the equilibrium distribution of this internal standard is similar to the equilibrium distribution of the species of interest.

Guaiacol was used as an internal standard, present at a mass fraction of 5%. All extractions were performed with equal masses of aqueous solution (with guaiacol present

at 5%) and ethyl acetate, each measured at 10 g. The extraction was performed with a 60 mL Kimax liquid-liquid extraction vessel. The organic extract was then dried with sodium sulfate so that the same GC injection and oven method could be used across all trials. Without any water, there is no need to account for a greater expansion upon vaporization.

To convert GC signal from this procedure into concentration values, new standards were made, using the liquid-liquid extraction process. Calibration curves were made from these standards; these curves differ from the set for organic solvents. Instead of concentrations plotted by signal, the ratio of the chemical concentration to the guaiacol concentration is plotted by the ratio of the chemical's integrated signal to guaiacol's integrated signal; this is shown in Figure 6.

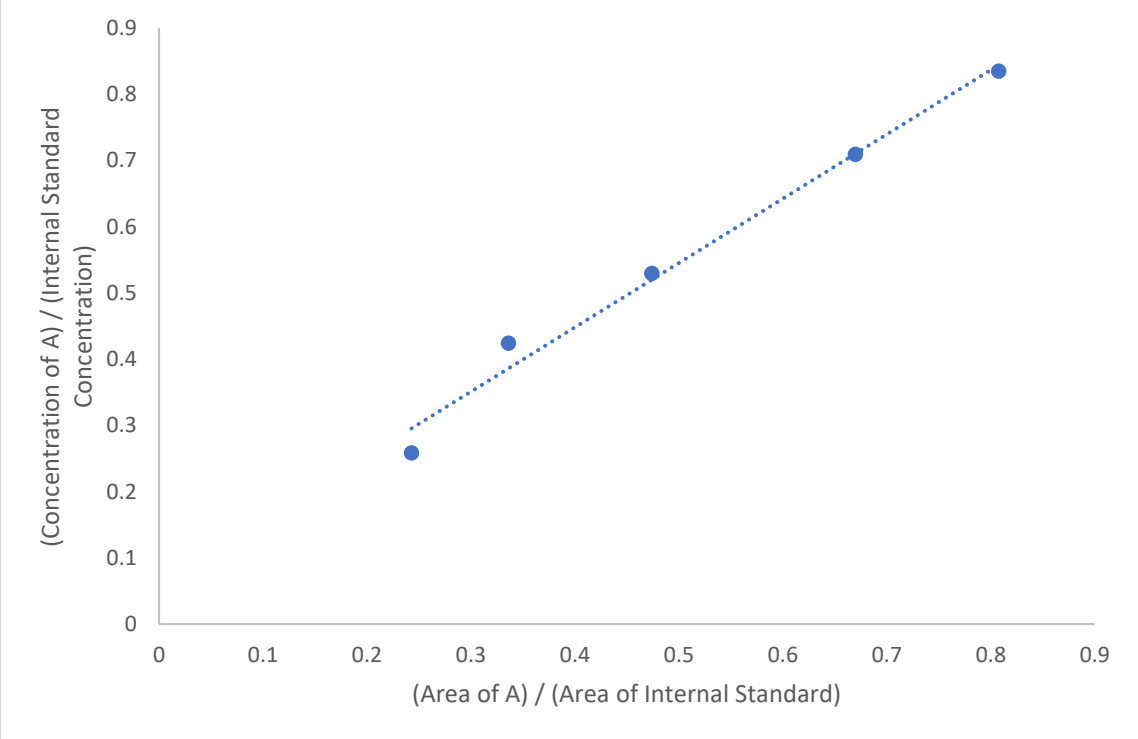

Figure 6. Example of calibration curve used for aqueous reactions. For both concentration and signal area, the ratios of analyte to internal standard are plotted.

This means that the concentration of a certain chemical is found by its proportion with reference to guaiacol, as opposed to the fraction of ethyl acetate solution it makes up. The solvent concentration in the sample does not affect the measured analyte concentration. This accounts for the distribution coefficient (assuming the distribution coefficient is equal for all species) and also gives concentrations that are unaffected by evaporation of solvent. Evaporation of solvent is not significant in the typical procedure, but the extra steps necessary for the aqueous method, particularly the drying with sodium sulfate, could lead to significant solvent evaporation.

CHAPTER III: HEAT AND MASS TRANSFER CONSIDERATIONS

The key results from these experiments are initial reaction rates. For the results to indicate differences in the reaction rates, the reaction must be kinetically controlled. Any heterogeneous catalyzed reaction taking place in catalytic particles can be broken down into five distinct steps.

First, material must diffuse from the bulk fluid to the catalyst surface. Second, adsorption must occur to bind the chemical species to the catalytic surface. Third, the reaction on the surface must occur. Fourth, the species desorbs from the surface, and fifth and last, the product diffuses back into the bulk fluid.

Temperature and concentration gradients can exist through the catalytic particle. These gradients change reaction rates with respect to radial position within the particle. The severity of these gradients can be quantified in a variety of ways. The Weisz-Prater number was used in these experiments to confirm no mass transfer limitations existed, as it is convenient to calculate with the gathered data. The calculation followed the description from Vannice.[31] A detailed description of the calculation is provided in Appendix B.

CHAPTER IV: SOLVENT SCREENING RESULTS

The results of most interest for this project can be depicted in a single plot, shown in Figure 7. This figure shows that a solvent effect is observed in phenol hydrogenation. The reaction rates in ethyl acetate, 1-butanol, and water do not differ by a statistically significant amount. However, for isopropanol and decalin, the hydrogenation rate is significantly higher. While this observed solvent effect does not change the order of magnitude of the reaction rate, it is significant, and it cannot be attributed to uncertainties in rate measurements.

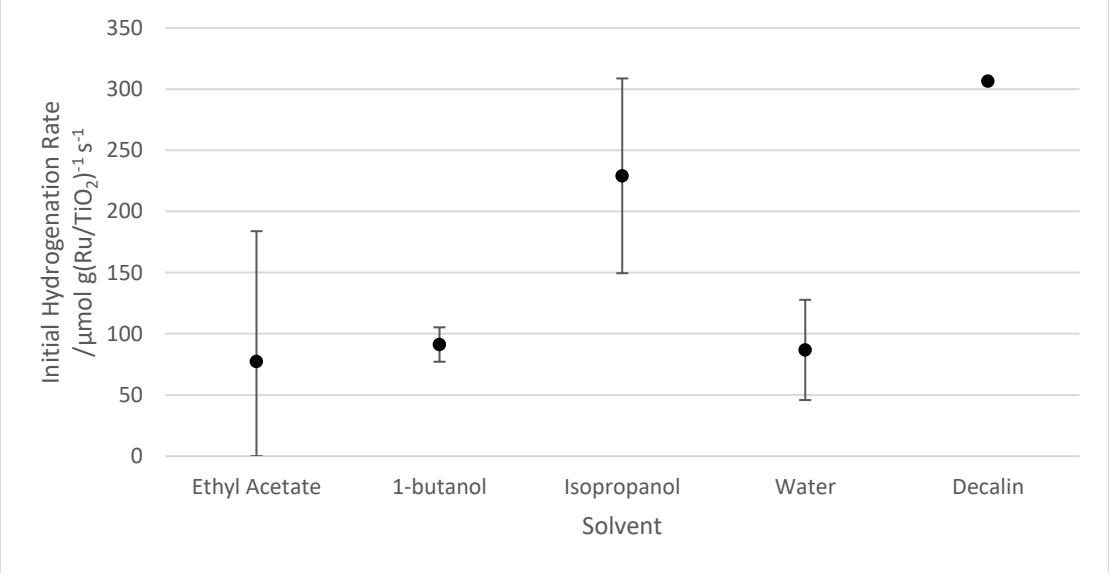

Figure 7. Initial hydrogenation rates in tested solvents. Reactions were performed with initial phenol concentration of 0.53 M in solvent, 33 bar hydrogen pressure, at 200 °C temperature setpoint. Error bars represent 95% confidence interval. Decalin point does not include error bars as only 1 data point was <30% conversion.

Something of note is that the two solvents giving higher reaction rates are not obviously chemically similar. 1-butanol and water yield a lower reaction rate than isopropanol; the presence of an alcohol group did not solely cause the increase in rate. Similarly, isopropanol is much more polar than decalin, but both led to a greater reaction rate.

In certain cases,[32–34] semi-empirical solvatochromic parameters have been able to explain observed solvent effects in reacting systems. Kamlet and Taft developed commonly used semi-empirical parameters to quantify effects from solvents based on the solvent's polarity (represented by π*), basicity (β), and acidity (α).[35] The parameters are based on the average of solvent effects on a variety of properties. This method, although being based in physical properties, is not specific enough to guarantee a correlation with a trend. The initial rates calculated from data gathered were plotted according to the acidity, basicity, and polarity of solvents predicted by the Kamlet-Taft method, and no r^2 value greater than 0.5 was found for single parameter correlations.

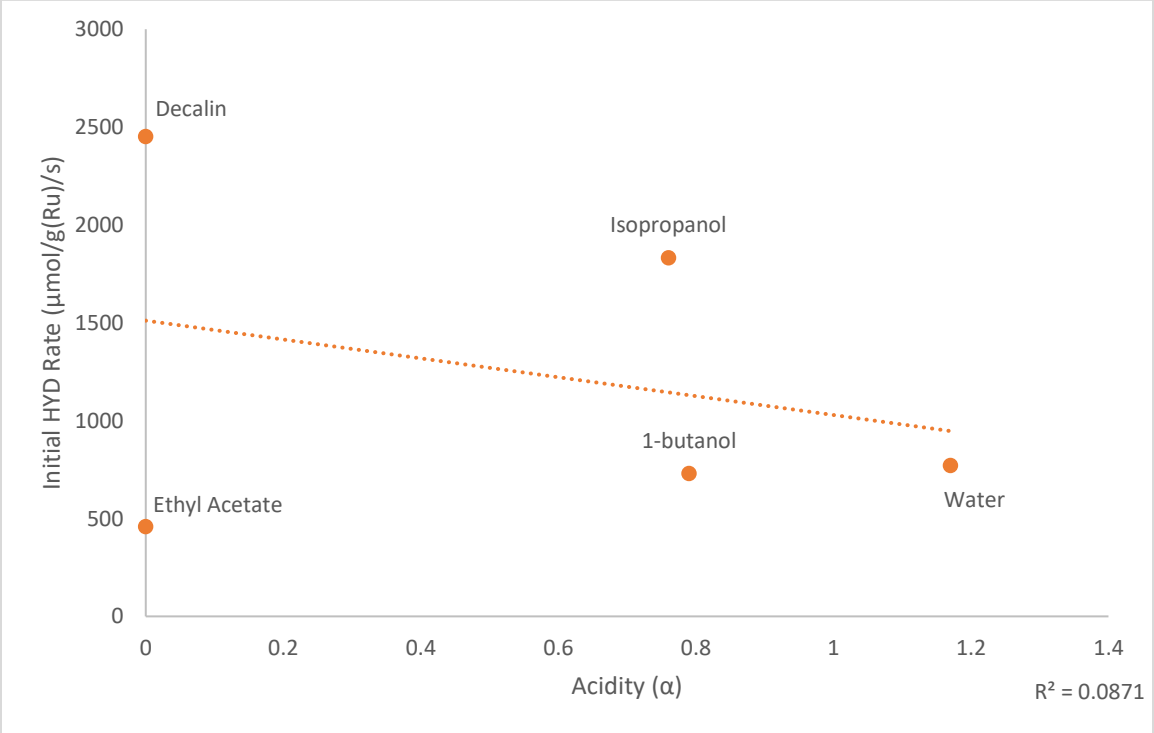

Figure 8. Initial hydrogenation rates plotted by solvent Kamlet-Taft α values. No correlation is observed.

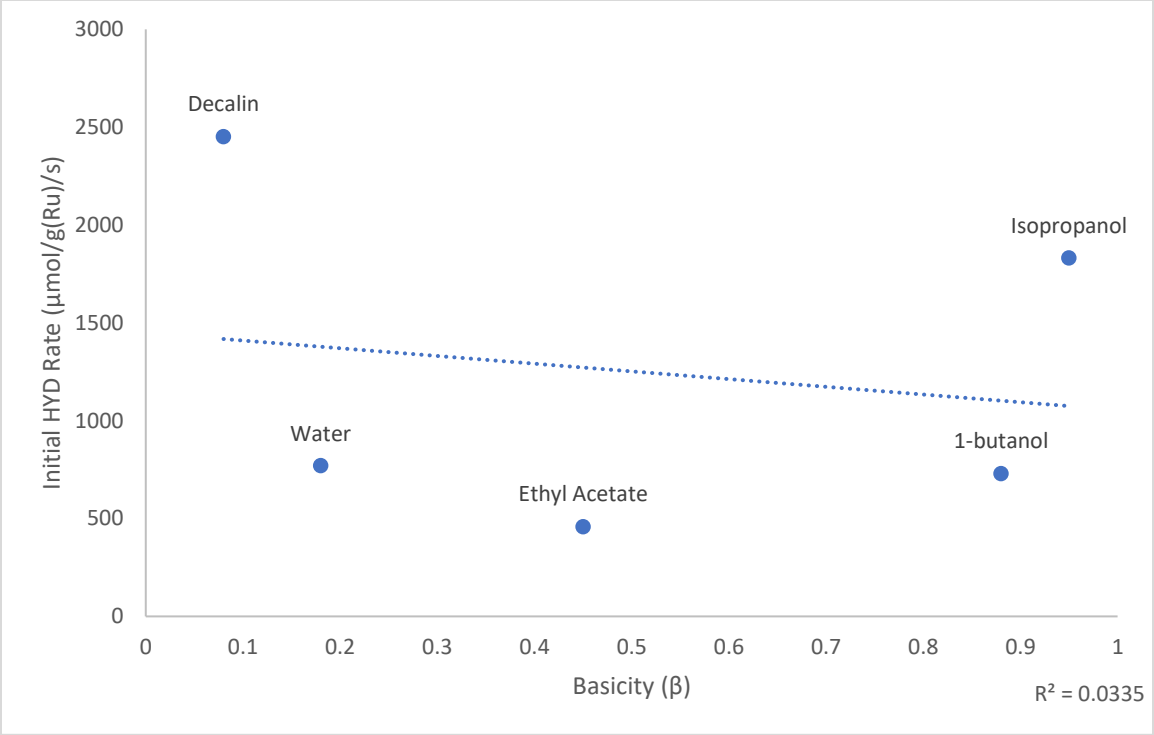

Figure 9. Initial hydrogenation rates plotted by solvent Kamlet-Taft β values. No correlation is observed.

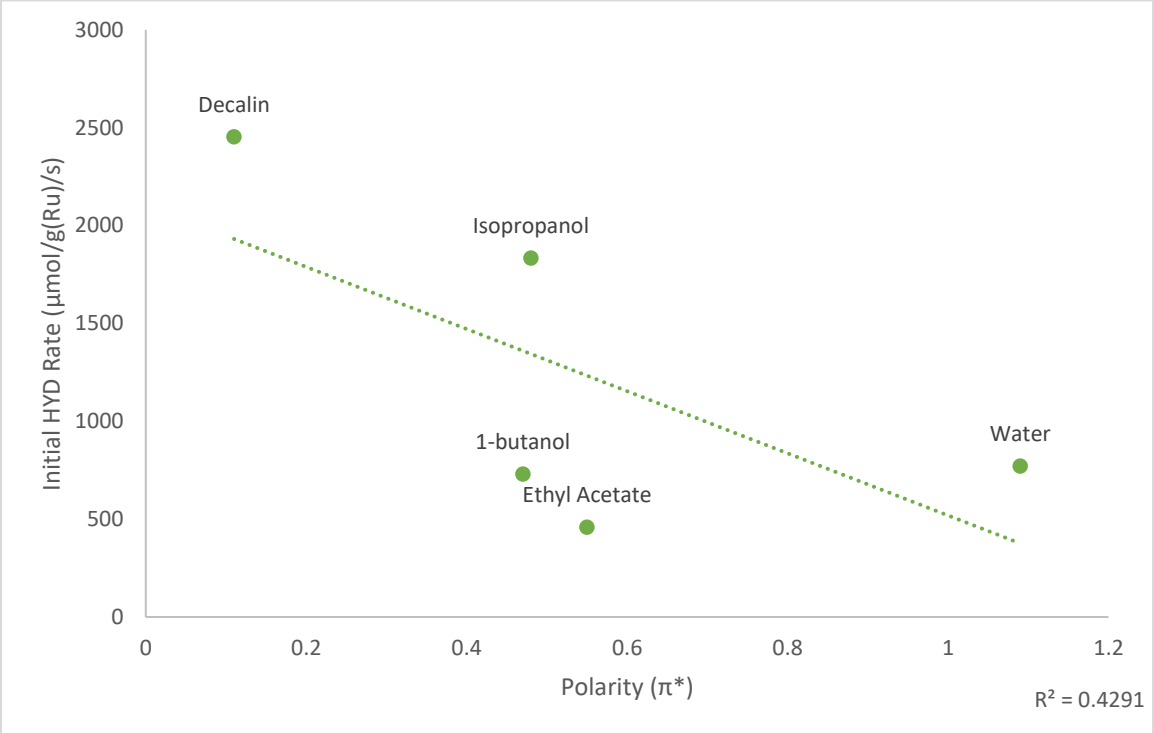

Figure 10. Initial hydrogenation rates plotted by solvent Kamlet-Taft π values. No correlation is observed.*

This is a limited analysis of the Kamlet-Taft parameters. It should be noted that there could be a significant trend according to the semi-empirical factors if a linear combination of two or all of the parameters was used to correlate reaction rates. It should also be noted that the parameters are not necessarily linearly independent; for example, basicity is not independent of polarity.[36] While a trend between a combination of Kamlet-Taft parameters could exist, the lack of an obvious trend makes the use of a more fundamental treatment of solvation effects attractive. As mentioned in the introduction, transition state theory allows a rigorous analysis of the effects of solvents on thermodynamic activities in reacting systems.

CHAPTER V: DISCUSSION

Chemical Potential and Activity

Reaction rates in ideal systems depend on concentrations, and often, particularly in the vapor phase, this is a convenient way to think of the driving forces of the reacting system. Thermodynamics ascertains that this is not strictly the case; reactions proceed to a minimum total Gibbs Free energy, leaving the partial molar Gibbs free energy (chemical potential, μ) as the driving force of a reaction.[37] Chemical potentials are affected by their environment through activities (a) which are defined according to Equation 8.[38]

$$\mu_i = \mu_i^\circ + RT\ln(a_i) \tag{8}$$

The superscript in the chemical potential on the right-hand side of the equation indicates this is a standard state chemical potential. The chosen reference state is arbitrary but will affect values of activities and how they are calculated. For an analysis of solvent effects in reacting systems, it is advantageous to take this reference state as a pure substance.[39] Solvent effects are observed in reactions due to interactions of chemical species. In an ideal solution, activities are equivalent to mole fractions. Activities quantify the non-ideality of a solution and are necessary for a rigorous thermodynamic analysis. The relationship between activities (a_i) and mole fractions (x_i) defines a coefficient (γ) that quantifies the degree of non-ideality.

$$a_i = \gamma_i x_i \tag{9}$$

Activities, which affect the driving force of chemical reactions, are a function of temperature, pressure, and composition of the system of interest (through both concentrations and chemical identities). Although there is a connection between concentration and activity, it is not trivial in non-ideal systems, and it is important to use

rigorous thermodynamics when analyzing non-ideal reactions. The unintuitive results observed show the effects of this relationship. Transition state theory provides a useful bridge between thermodynamics and kinetics, with relatively simple rate expressions.

Transition State Theory Rate Equation for a Bimolecular Liquid Phase Reaction

The system analyzed in TST here is a bimolecular liquid phase reaction: A + B → $\{X_f\}$. The curly braces on X_f indicate that the quantity is an activated complex and will not exist stably in solution. This model does not strictly consider the reactants to be adsorbed to a surface; however, if a solvent effect is observed in a surface reaction, it can be said that the reactants "feel" the effects of the solvent like a liquid.[11]

We begin with the common TST statement that the reaction rate expressed in moles per volume per time is proportional to the frequency of activated complexes crossing the critical dividing surface to become products (ν) multiplied by the concentration of transition states in the unit volume ($C^{\ddagger}$). Concentration is converted to mole fraction so equations with activity can be combined.

$$r = \nu\, C^{\ddagger} = \nu\, x^{\ddagger}\, {}^{N}/_{V} \tag{10}$$

A key assumption from TST is that the transition states, or activated complexes, are in thermal equilibrium with the reactants.[38] An equilibrium constant between reactants and activated complexes can be written for a non-ideal environment.

$$K = \frac{a^{\ddagger}}{a_A a_B} = \frac{\gamma^{\ddagger}}{\gamma_A \gamma_B} \frac{x^{\ddagger}}{x_A x_B} = \gamma^{\ddagger} \frac{x^{\ddagger}}{a_A a_B} \tag{11}$$

This can be rearranged and substituted into Equation 10.

$$r = \nu\, \frac{K}{\gamma^{\ddagger}} \frac{N}{V} a_A a_B \tag{12}$$

Transition state theory gives a way to relate the equilibrium constant built from activities to the equilibrium constant built from partition functions, which is of direct use in a

reaction rate of ideal gases.[38] For ideal gases, the entire equilibrium constant can be built from partition functions, which have exact definitions. For a non-ideal environment, there is only one partition function for which exact information is known.

$$K = z_{rc} K^{\ddagger} \tag{13}$$

The partition function expressed here is for the motion along the reaction coordinate. It can be expressed as a vibration and takes on the form of a vibrational partition function.

$$z_{rc} = \frac{1}{1-\exp\left(-{}^{h\nu}/_{k_b T}\right)} \tag{14}$$

Although this motion is depicted as a vibration, assumptions of TST dictate that no activated complexes crossing the critical dividing surface move backwards along the reaction coordinate. Therefore, the vibration that corresponds to movement along this reaction coordinate cannot have a real restoring force, indicating the characteristic frequency is imaginary and the limit of the partition function can be taken as the characteristic frequency goes to zero. A Taylor series truncated after the first two terms gives the solution to Equation 14.

$$\lim_{\nu \to 0} \frac{1}{1-\exp\left(-{}^{h\nu}/_{k_b T}\right)} = \frac{1}{1-\left(1-{}^{h\nu}/_{k_b T}\right)} = {}^{k_b T}/_{h\nu} = z_{rc} \tag{15}$$

The remaining equilibrium constant on the right-hand side of Equation 13 can be related to the Gibbs Free energy change for forming the transition state.

$$K^{\ddagger} = e^{-\frac{\Delta G^{\ddagger}}{RT}} \tag{16}$$

Combining Equations 12, 13, 15, and 16 gives the complete reaction rate equation.

$$r = \frac{k_b T}{h} e^{-\frac{\Delta G^{\ddagger}}{RT}} \frac{1}{\gamma^{\ddagger}} \frac{N}{V} a_A a_B \tag{17}$$

Constant terms can be gathered to give an apparent rate constant $k_a = \frac{k_b T}{h} e^{-\frac{\Delta G^{\ddagger}}{RT}}$, leaving the final concise equation.

$$r = k_a \frac{1}{\gamma^{\ddagger}} \frac{N}{V} a_A a_B \tag{18}$$

This is the concise general equation from transition state theory for a bimolecular reaction in a non-ideal environment. If all activity coefficients are assumed to be unity, as in an ideal solution, this expression reduces to be in terms of concentrations. In a non-ideal environment, such as the one studied here, the coefficients do not reduce to unity. In fact, for some liquid phase reactions, the term of activity coefficients for reactants and the transition state may differ by orders of magnitude when predicted by UNIFAC.[39]

TST for Phenol Hydrogenation

Equation 18 is true for an elementary reaction experiencing intermolecular forces. There are five elementary steps to a reaction occurring on a surface.

1. Diffusion of the reactant from the bulk to the surface
2. Adsorption of the reactant to the surface
3. Reaction on the surface, which may occur in many elementary steps
4. Desorption of product from the surface
5. Diffusion of the product from the surface to the bulk

Of the 5 steps to a heterogeneous catalytic reaction, steps 2 and 4 are usually the only steps that have a transition state experiencing intermolecular forces from the solvent. Typically, a fluid is not in close enough proximity to surface species, like those in step 3, to have an observable effect; the ratio of activity coefficients in the equation for step 3 can be assumed to be unity.[11] Steps 1 and 5 involve transport, and do not have transition states or follow rate equations. For steps 2 and 4, the adsorbing or desorbing transition

state feels effects of the solvent more as it is extended into the fluid from the surface. Thus, the ratio of activity coefficients is significant. Therefore, solvent effects will be observed when the adsorbing or desorbing steps have a significant degree of rate control. For the hydrogenation of phenol, the potential rate determining steps are adsorption of hydrogen, adsorption of phenol, and desorption of cyclohexenol. Only desorption of cyclohexenol is considered as other species like cyclohexanol or cyclohexane are farther down the reaction sequence (Figure 4) and would not affect initial rates. It should be noted that any cyclohexenol in solution quickly tautomerizes to cyclohexanone, which is detected in the product. This tautomerization may happen in the bulk phase, or on the surface before the desorption occurs. For the work here, the tautomerization is assumed to happen in the bulk phase for simplicity of communication, but this assumption needs to be rigorously investigated in future work.

Effect of Hydrogen

The rate expression should include a term for the activity of hydrogen. If the entry step of dissociative hydrogen adsorption were the rate determining step, as is the case for the hydrogenation of cyclohexene on Pt,[11] then the concentration of hydrogen in the liquid phase would be directly observable in the final rate equation. With different solvents used, this liquid hydrogen concentration is different in each.

To calculate hydrogen concentration in various solvents, Henry's constants were used. Values for the constants of hydrogen in organic solvents were found empirically by Luehring et. al.[40] and used to calculate initial hydrogen concentration in solution. Luehring et. al. measured constants for organic solvents. For water, empirical data with a regressed correlation[41] was used.

The initial rate of reaction is plotted according to the concentration of hydrogen in the liquid phase in Figure 11.

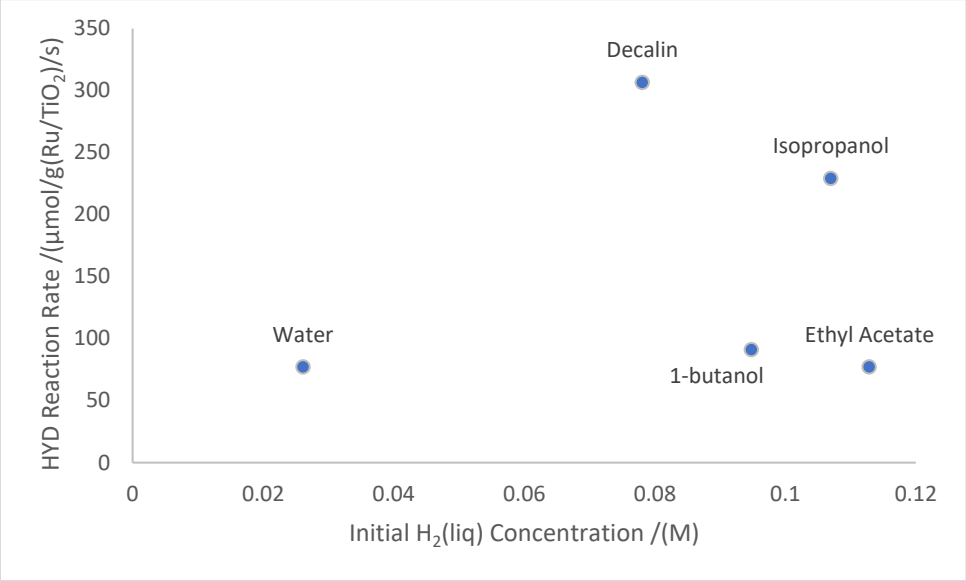

Figure 11. Initial HYD rates by initial hydrogen concentrations in liquid. Initial hydrogen concentrations calculated from empirical Henry's coefficients.

If the concentration of hydrogen was retained in the final rate equation, it would have the form of Equation 2, as in the hydrogenation of cyclohexene on Pt.[11]

$$r_{Pt} = kC_{H_2} \tag{2}$$

Data following a rate equation like Equation 2 would show a linear relationship in Figure 11. No relationship is observed, so the data shows that dissociative adsorption of hydrogen is not the rate determining step of phenol hydrogenation.

Phenol Adsorption and Cyclohexenol Desorption

From the above discussion, we believe that hydrogen activity contributes to the rate expression; its activity coefficient does not separate and fortuitously cancel with an activity coefficient of a kinetically relevant transition state. The rate equation can then be simplified by absorbing hydrogen activity into the apparent rate constant. This is possible

as hydrogen pressure, and thus activity, was constant for all trials examined here. This leaves two possible rate expressions, one if the rate determining step was phenol adsorption, and one if the rate determining step was cyclohexenol desorption.

$$r_{ads} = k_a \frac{N}{V} \frac{\gamma_{Ph}}{\gamma^{\ddagger}} x_{Ph} \tag{19}$$

$$r_{des} = k_a \frac{N}{V} \frac{\theta_{Cyclohexenol}}{\gamma^{\ddagger}} \tag{20}$$

The desorption rate is written in terms of fractional coverage of the surface, as the elementary step here is an adsorbed cyclohexenol molecule desorbing from the surface. This is the equation in the simplest form – the fractional coverage of cyclohexenol can be related to activity of phenol.

A microkinetic model and DFT calculations were recently used to model benzene hydrogenation on many catalytic surfaces.[42] The group determined that on a Ru(0001) surface, the degree of rate control for cyclohexene desorption was >0.9. Other elementary steps with significant degrees of rate control are cyclohexene formation and cyclohexane formation with degrees of ~0.7 and ~0.4 respectively. If cyclohexene desorption is assumed to be the rate-determining step in benzene hydrogenation, a solvent effect could be observed. Analogously, if a desorbing cyclohexenol structure is similar to a desorbing cyclohexene structure, the desorption exit step could be the rate determining step in phenol hydrogenation as it is in benzene hydrogenation.

Making the assumption that desorption is the rate determining step, we return to the rate expression for desorption, as expressed in Equation 20. If the degrees of rate control for elementary steps are similar to benzene hydrogenation, the adsorption rate can be assumed to be quasi-equilibrated with the adsorption of phenol. Thus, a new rate constant can be defined, and the driving force of the reaction can be attributed to phenol.

$$r = r_{des} = k'_a \frac{N}{V} \frac{\gamma_{Phenol}}{\gamma^{\ddagger}_{des\_Cyclohexenol}} C^{\alpha}_{Phenol} \quad (21)$$

This is the concise statement of the rate equation. When the rate equations are compiled and the rate is expressed in concentration of phenol, the reaction order can change depending on the mechanism of reaction. As that is unknown here, the order is expressed as an unknown order, alpha (α). Previous research has reported the order of hydrogenation with respect to phenol to be fractional at low phenol concentration due to coverage of the surface by phenol fragments.[20]

The most important piece of this equation is that the solvent effect can be captured into a single term by the ratio of the activity coefficient of phenol to the activity coefficient of the activated complex for cyclohexenol desorption.

Estimating the Activity Coefficient Ratio

The activity of a species in solution depends on temperature, composition, and chemical identity of the species in solution.[43] Activities can be estimated using many different methods, one of which is the Universal Quasichemical Functional-group Activity Coefficients method, UNIFAC. This method estimates activities by counting contributions from functional groups of the mixture. The contributions were determined from empirical values regressed according to the composition of functional groups. The activity coefficients of phenol and cyclohexenol (representing the transition state) were calculated for each solvent system, and the ratio was plotted on the same chart as the initial rates to determine if there was a correlation. Activity coefficients were calculated for a system consisting of phenol present at the average mole fraction of the reaction, a transition state concentration equal to a tenth of the phenol mole fraction, and

solvent making up the rest of the system. The temperature was calculated as a time-average of the temperature of the reactor (as shown in Figure 5) with a value of 164 °C.

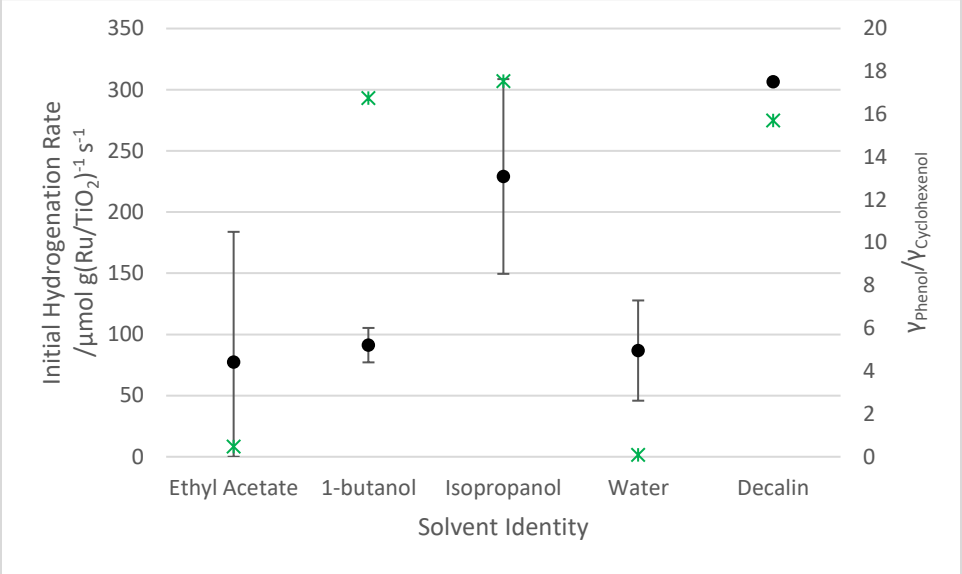

Figure 12. Activity coefficient ratio from TST expression plotted with initial rates. Activity coefficient ratios shown by green asterisks calculated close to 5 mol% (exact composition depending on solvent) at average of reactor temperature. Rates shown as black circles were measured at 33 bar hydrogen, 200 degC setpoint. Error bars represent 95% confidence intervals.

Barring the ratio calculated for butanol, there is a clear trend between activity coefficient ratio and measured initial rate; the rates measured in decalin and isopropanol correspond to activity coefficient ratios calculated between 15 and 18, whereas the rates measured in ethyl acetate and water correspond to activity coefficient ratios calculated to be less than unity. The rate in butanol does not match the trend. The measured rate is similar to ethyl acetate and water, while the calculated ratio is similar to isopropanol and decalin. This outlier should be noted and investigated as a part of future work.

The results above have confidence intervals shown which estimate the error in the measured rates. The error in the value of the activity coefficient ratio is of course, also of interest.

Activity coefficients were also calculated for a temperature of 200 °C with compositions 5 mol% phenol, 1 mol% transition state, and 94 mol% solvent. Under these conditions, the activity coefficient ratio was calculated for a cyclohexanone and a cyclohexenol transition state. The results are plotted similarly to Figure 12.

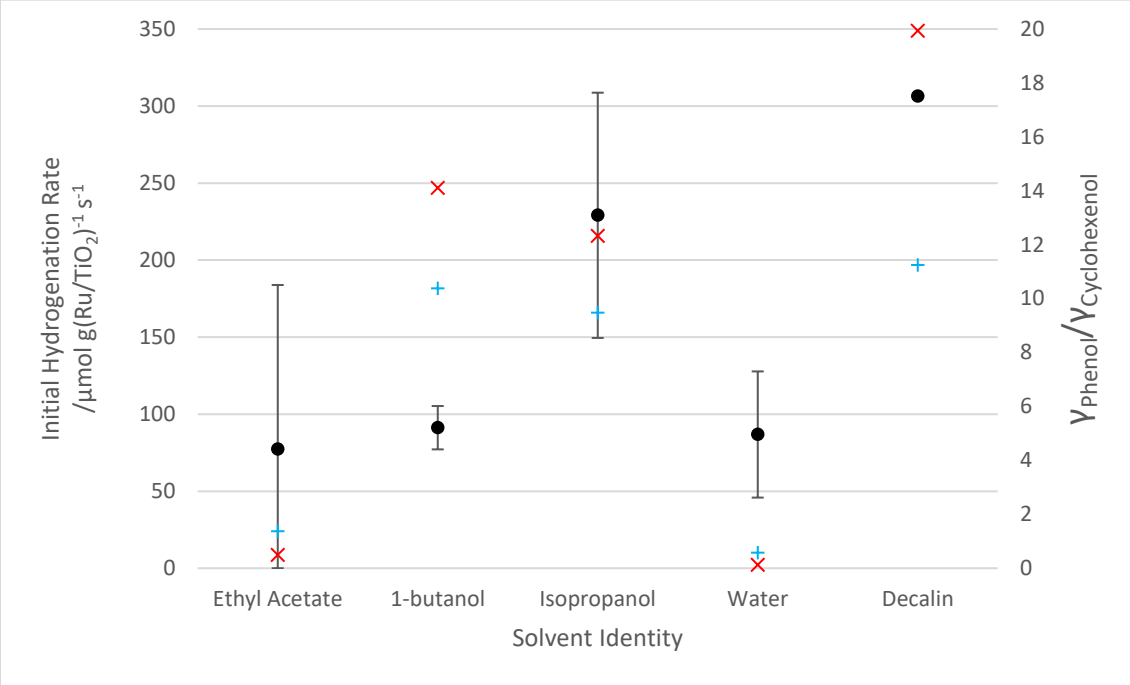

Figure 13. Activity coefficient ratio from TST expression plotted with initial rates. Activity coefficients calculated at 5 mol% phenol, 1 mol% TS, and 94 mol% solvent. Activity coefficient ratios shown by red X for cyclohexenol TS, blue + for cyclohexanone TS. Rates shown as black circles were measured at 33 bar hydrogen, 200 degC setpoint. Error bars represent 95% confidence intervals.

Although values can differ when the transition state, composition, and temperature are changed, the trend between points at different conditions remains the same. This illustrates that the activity coefficient ratio derived from transition state theory can help explain solvent effects observed.

CHAPTER VI: CONCLUSION & RECOMMENDATIONS FOR FUTURE WORK

The work presented here shows that there is a significant solvent effect from some of the solvents examined here in the hydrogenation of phenol on a Ru/TiO_2 catalyst. These solvent effects can be exploited to increase or decrease the rate of hydrogenation, depending on what is desired from the reaction. If saturated products are desired, a solvent could be chosen to increase the hydrogenation rate, whereas if hydrogenolysis products were desired, the hydrogenation rate could be decreased through solvent choice to increase selectivity to the DDO pathway.

Future work in this project could investigate the activity coefficient ratio more. UNIFAC is one method of many that calculates activity coefficients and can have errors associated with values derived from it depending on the system. The sensitivity of the ratio with temperature and composition should also be known. For the experimental setup in this work, the apparent temperature is unknown. Future experiments would benefit from a known temperature and other more precise experiments.

With more precise experiments, another area of interest is the nature of the transition state. The rate determining step should be determined rigorously, to verify if it is desorption. Assuming it is, the nature of the transition state, whether it is similar to cyclohexanone or cyclohexenol, is of interest. The mechanism around the rest of the reaction pathway is also unknown, and there would be benefit to identifying it.

Other worthwhile work with this project would be expanding the dataset by running the reaction in more solvents to build a more general trend. The difference in initial rate between isopropanol and 1-butanol indicate that the solvent effect observed is not trivial. A wider range of solvents could help show the chemical mechanism of the effect.

WORKS CITED

(1) Daioglou, V.; Doelman, J. C.; Wicke, B.; Faaij, A.; van Vuuren, D. P. Integrated Assessment of Biomass Supply and Demand in Climate Change Mitigation Scenarios. *Global Environmental Change* **2019**, *54*, 88–101. https://doi.org/10.1016/j.gloenvcha.2018.11.012.

(2) Uría-Martínez, R.; Leiby, P. N.; Brown, M. L. Energy Security Role of Biofuels in Evolving Liquid Fuel Markets. *Biofuels, Bioproducts and Biorefining* **2018**, *12* (5), 802–814. https://doi.org/10.1002/bbb.1891.

(3) Nong, D.; Escobar, N.; Britz, W.; Börner, J. Long-Term Impacts of Bio-Based Innovation in the Chemical Sector: A Dynamic Global Perspective. *Journal of Cleaner Production* **2020**, *272*, 122738. https://doi.org/10.1016/j.jclepro.2020.122738.

(4) *Glossary:Carbon dioxide equivalent*. https://ec.europa.eu/eurostat/statistics-explained/index.php?title=Glossary:Carbon_dioxide_equivalent (accessed 2022-04-24).

(5) Sustainable Forestry Initiative. SFI. https://forests.org

(6) Anex, R. P.; Aden, A.; Kazi, F. K.; Fortman, J.; Swanson, R. M.; Wright, M. M.; Satrio, J. A.; Brown, R. C.; Daugaard, D. E.; Platon, A.; Kothandaraman, G.; Hsu, D. D.; Dutta, A. Techno-Economic Comparison of Biomass-to-Transportation Fuels via Pyrolysis, Gasification, and Biochemical Pathways. *Fuel* **2010**, *89*, S29–S35. https://doi.org/10.1016/j.fuel.2010.07.015.

(7) Di Blasi, C. Combustion and Gasification Rates of Lignocellulosic Chars. *Progress in Energy and Combustion Science* **2009**, *35* (2), 121–140. https://doi.org/10.1016/j.pecs.2008.08.001.

(8) Bridgwater, A. V. Review of Fast Pyrolysis of Biomass and Product Upgrading. *Biomass and Bioenergy* **2012**, *38*, 68–94. https://doi.org/10.1016/j.biombioe.2011.01.048.

(9) Hoang Pham, L. K.; Vi Tran, T. T.; Kongparakul, S.; Reubroycharoen, P.; Ding, M.; Guan, G.; Vo, D.-V. N.; Jaiyong, P.; Youngvises, N.; Samart, C. Data-Driven Prediction of Biomass Pyrolysis Pathways toward Phenolic and Aromatic Products. *Journal of Environmental Chemical Engineering* **2021**, *9* (2), 104836. https://doi.org/10.1016/j.jece.2020.104836.

(10) Mellmer, M. A.; Sener, C.; Gallo, J. M. R.; Luterbacher, J. S.; Alonso, D. M.; Dumesic, J. A. Solvent Effects in Acid-Catalyzed Biomass Conversion Reactions. *Angewandte Chemie International Edition* **2014**, *53* (44), 11872–11875. https://doi.org/10.1002/anie.201408359.

(11) Madon, R. J.; Iglesia, E. Catalytic Reaction Rates in Thermodynamically Non-Ideal Systems. *Journal of Molecular Catalysis A: Chemical* **2000**, *163* (1–2), 189–204. https://doi.org/10.1016/S1381-1169(00)00386-1.

(12) Madon, R. J.; O'Connell, J. P.; Boudart, M. Catalytic Hydrogenation of Cyclohexene: Part II. Liquid Phase Reaction on Supported Platinum in a Gradientless Slurry Reactor. *AIChE Journal* **1978**, *24* (5), 904–911. https://doi.org/10.1002/aic.690240516.

(13) Gonzo, E. E.; Boudart, M. Catalytic Hydrogenation of Cyclohexene: 3. Gas-Phase and Liquid-Phase Reaction on Supported Palladium. *Journal of Catalysis* **1978**, *52* (3), 462–471. https://doi.org/10.1016/0021-9517(78)90352-4.

(14) Singh, N.; Lee, M.-S.; Akhade, S. A.; Cheng, G.; Camaioni, D. M.; Gutiérrez, O. Y.; Glezakou, V.-A.; Rousseau, R.; Lercher, J. A.; Campbell, C. T. Impact of PH on Aqueous-Phase Phenol Hydrogenation Catalyzed by Carbon-Supported Pt and Rh. *ACS Catalysis* **2018**. https://doi.org/10.1021/acscatal.8b04039.

(15) Hensley, A. J. R.; Bray, J.; Shangguan, J.; Chin, Y.-H. (Cathy); McEwen, J.-S. Catalytic Consequences of Hydrogen Addition Events and Solvent-Adsorbate Interactions during Guaiacol-H2 Reactions at the H2O-Ru(0 0 0 1) Interface. *Journal of Catalysis* **2021**, *395*, 467–482. https://doi.org/10.1016/j.jcat.2020.09.034.

(16) Sjostrom, E. *Wood Chemistry: Fundamentals and Applications*; Gulf Professional Publishing, 1993.

(17) Parkhurst, J.; Huibers, D. T. A.; Jones, M. W. Production of Phenol from Lignin. *Am. Chem. Soc., Div. Pet. Chem., Prepr.; (United States)* **1980**, *25:3*.

(18) Furimsky, E. Catalytic Hydrodeoxygenation. *Applied Catalysis A: General* **2000**, *199* (2), 147–190. https://doi.org/10.1016/S0926-860X(99)00555-4.

(19) Nelson, R. C.; Baek, B.; Ruiz, P.; Goundie, B.; Brooks, A.; Wheeler, M. C.; Frederick, B. G.; Grabow, L. C.; Austin, R. N. Experimental and Theoretical Insights into the Hydrogen-Efficient Direct Hydrodeoxygenation Mechanism of Phenol over Ru/TiO $_2$. *ACS Catal.* **2015**, *5* (11), 6509–6523. https://doi.org/10.1021/acscatal.5b01554.

(20) Stück, D. Reaction Kinetics Analysis of C-O Hydrogenoloysis in Phenol and 5-Hydroxymethylfurfural. Master of Science, University of Maine, 2019.

(21) Khlewee, A. M. Characterization of Catalysts for Hydrodeoxygenation of Bio-Oils Using Phenol as a Model Compound, The University of Maine, 2017.

(22) Newman, C.; Zhou, X.; Goundie, B.; Ghampson, I. T.; Pollock, R. A.; Ross, Z.; Wheeler, M. C.; Meulenberg, R. W.; Austin, R. N.; Frederick, B. G. Effects of Support Identity and Metal Dispersion in Supported Ruthenium Hydrodeoxygenation Catalysts. *Applied Catalysis A: General* **2014**, *477*, 64–74. https://doi.org/10.1016/j.apcata.2014.02.030.

(23) Huber, G. W.; Chheda, J. N.; Barrett, C. J.; Dumesic, J. A. Production of Liquid Alkanes by Aqueous-Phase Processing of Biomass-Derived Carbohydrates. *Science* **2005**. https://doi.org/10.1126/science.1111166.

(24) Shangguan, J.; Pfriem, N.; Chin, Y.-H. (Cathy). Mechanistic Details of CO Bond Activation in and H-Addition to Guaiacol at Water-Ru Cluster Interfaces. *Journal of Catalysis* **2019**, *370*, 186–199. https://doi.org/10.1016/j.jcat.2018.11.036.

(25) Yoon, Y.; Rousseau, R.; Weber, R. S.; Mei, D.; Lercher, J. A. First-Principles Study of Phenol Hydrogenation on Pt and Ni Catalysts in Aqueous Phase. *J. Am. Chem. Soc.* **2014**, *136* (29), 10287–10298. https://doi.org/10.1021/ja501592y.

(26) Wang, X.; Zhu, S.; Wang, S.; Wang, J.; Fan, W.; Lv, Y. Ni Nanoparticles Entrapped in Nickel Phyllosilicate for Selective Hydrogenation of Guaiacol to 2-Methoxycyclohexanol. *Applied Catalysis A: General* **2018**, *568*, 231–241. https://doi.org/10.1016/j.apcata.2018.10.009.

(27) Kim, H.; Yang, S.; Lim, Y. H.; Lee, J.; Ha, J.-M.; Kim, D. H. Enhancement in the Metal Efficiency of Ru/TiO2 Catalyst for Guaiacol Hydrogenation via Hydrogen Spillover in the Liquid Phase. *Journal of Catalysis* **2022**, *410*, 93–102. https://doi.org/10.1016/j.jcat.2022.04.017.

(28) Wang, H.; Male, J.; Wang, Y. Recent Advances in Hydrotreating of Pyrolysis Bio-Oil and Its Oxygen-Containing Model Compounds. *ACS Catal.* **2013**, *3* (5), 1047–1070. https://doi.org/10.1021/cs400069z.

(29) Chiu, C.; Genest, A.; Borgna, A.; Rösch, N. Hydrodeoxygenation of Guaiacol over Ru(0001): A DFT Study. *ACS Catal.* **2014**, *4* (11), 4178–4188. https://doi.org/10.1021/cs500911j.

(30) Tavana, J.; Faysal, A.; Vithanage, A.; Gramlich, W. M.; Schwartz, T. J. Pathway to Fully-Renewable Biobased Polyesters Derived from HMF and Phenols. *Polym. Chem.* **2022**, *13* (9), 1215–1227. https://doi.org/10.1039/D1PY01441B.

(31) Vannice, M. . A. *Kinetics of Catalytic Reactions*, 1st ed.; Springer Science+Business Media, Inc., 2005.

(32) Romo, J. E.; Miller, K. C.; Sundsted, T. L.; Job, A. L.; Hoo, K. A.; Wettstein, S. G. The Effect of Solvent Polarity on Autocatalytic Furfural Production Confirmed by Multivariate Statistical Analysis. *ChemCatChem* **2019**, *11* (19), 4715–4719. https://doi.org/10.1002/cctc.201900969.

(33) Doherty, T. V.; Mora-Pale, M.; Foley, S. E.; Linhardt, R. J.; Dordick, J. S. Ionic Liquid Solvent Properties as Predictors of Lignocellulose Pretreatment Efficacy. *Green Chem.* **2010**, *12* (11), 1967–1975. https://doi.org/10.1039/C0GC00206B.

(34) Fathalla, M. F. Solvent Effect on the Alkaline Hydrolysis of 2-Thiophenyl- 3,5-Dinitropyridine. *International Journal of Chemical Kinetics* **2006**, *38* (3), 159–165. https://doi.org/10.1002/kin.20146.

(35) Kamlet, M. J.; Abboud, J. L. M.; Abraham, M. H.; Taft, R. W. Linear Solvation Energy Relationships. 23. A Comprehensive Collection of the Solvatochromic Parameters, .Pi.*, .Alpha., and .Beta., and Some Methods for Simplifying the Generalized Solvatochromic Equation. *J. Org. Chem.* **1983**, *48* (17), 2877–2887. https://doi.org/10.1021/jo00165a018.

(36) Jessop, P. G.; Jessop, D. A.; Fu, D.; Phan, L. Solvatochromic Parameters for Solvents of Interest in Green Chemistry. *Green Chem.* **2012**, *14* (5), 1245–1259. https://doi.org/10.1039/C2GC16670D.

(37) Smith, J. M.; Van Ness, H. C.; Abbott, M. M.; Swihart, M. T. *Introduction to Chemical Engineering Thermodynamics*, 8th ed.; McGraw-Hill Education: New York, NY, 2018.

(38) Levine, I. N. *Physical Chemistry*, 6th ed.; McGraw Hill Education: India.

(39) Schwartz, T. J.; Bond, J. Q. Leveraging De Donder Relations for a Thermodynamically Rigorous Analysis of Reaction Kinetics in Liquid Media. *Journal of Catalysis* **2021**, *404*, 687–705. https://doi.org/10.1016/j.jcat.2021.09.026.

(40) Luehring, P.; Schumpe, A. Gas Solubilities (Hydrogen, Helium, Nitrogen, Carbon Monoxide, Oxygen, Argon, Carbon Dioxide) in Organic Liquids at 293.2 K. *J. Chem. Eng. Data* **1989**, *34* (2), 250–252. https://doi.org/10.1021/je00056a029.

(41) Yaws, C. L. *Yaws' Critical Property Data for Chemical Engineers and Chemists*, 4th ed.; Knovel, 2017.

(42) He, H.; Meyer, R. J.; Rioux, R. M.; Janik, M. J. Catalyst Design for Selective Hydrogenation of Benzene to Cyclohexene through Density Functional Theory and Microkinetic Modeling. *ACS Catal.* **2021**, *11* (19), 11831–11842. https://doi.org/10.1021/acscatal.1c02630.

(43) Sandler, S. I. *Chemical and Engineering Thermodynamics*, 3rd ed.; John Wiley & Sons, Inc., 1999.

(44) Ternan, M. The Diffusion of Liquids in Pores. *The Canadian Journal of Chemical Engineering* **1987**, *65*, 244–249.

(45) Satterfield, C. N.; Colton, C. K.; Pitcher, W. H. Restricted Diffusion within Fine Pores. *AIChE J.* **1973**, *19*, 628–635.

(46) Lorenc-Grabowska, E. Effect of Micropore Size Distribution on Phenol Adsorption on Steam Activated Carbons. *Adsorption* **2016**, *22* (4–6), 599–607. https://doi.org/10.1007/s10450-015-9737-x.

(47) Mahdavi-Shakib, A.; Husremovic, S.; Ki, S.; Glynn, J.; Babb, L.; Sempel, J.; Stavrinoudis, I.; Arce-Ramos, J.-M.; Nelson, R.; Grabow, L. C.; Schwartz, T. J.; Frederick, B. G.; Austin, R. N. Titania Surface Chemistry and Its Influence on Supported Metal Catalysts. *Polyhedron* **2019**, *170*, 41–50. https://doi.org/10.1016/j.poly.2019.05.012.

(48) Wilke, C. R.; Chang, P. Correlation of Diffusion Coefficients in Dilute Solutions. *AIChE J.* **1955**, *1*, 264–270.

APPENDICES

APPENDIX A: CALIBRATION CURVES

The calibration curves used to convert integrated signal from the GC-FID output to a concentration are included below.

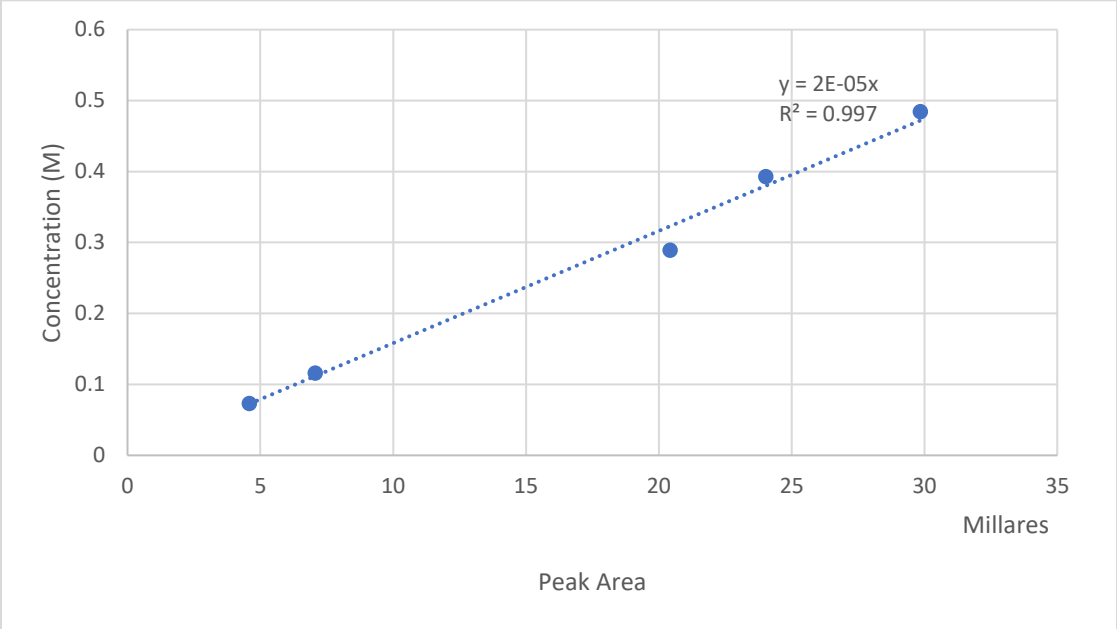

Figure A1. Phenol calibration curve.

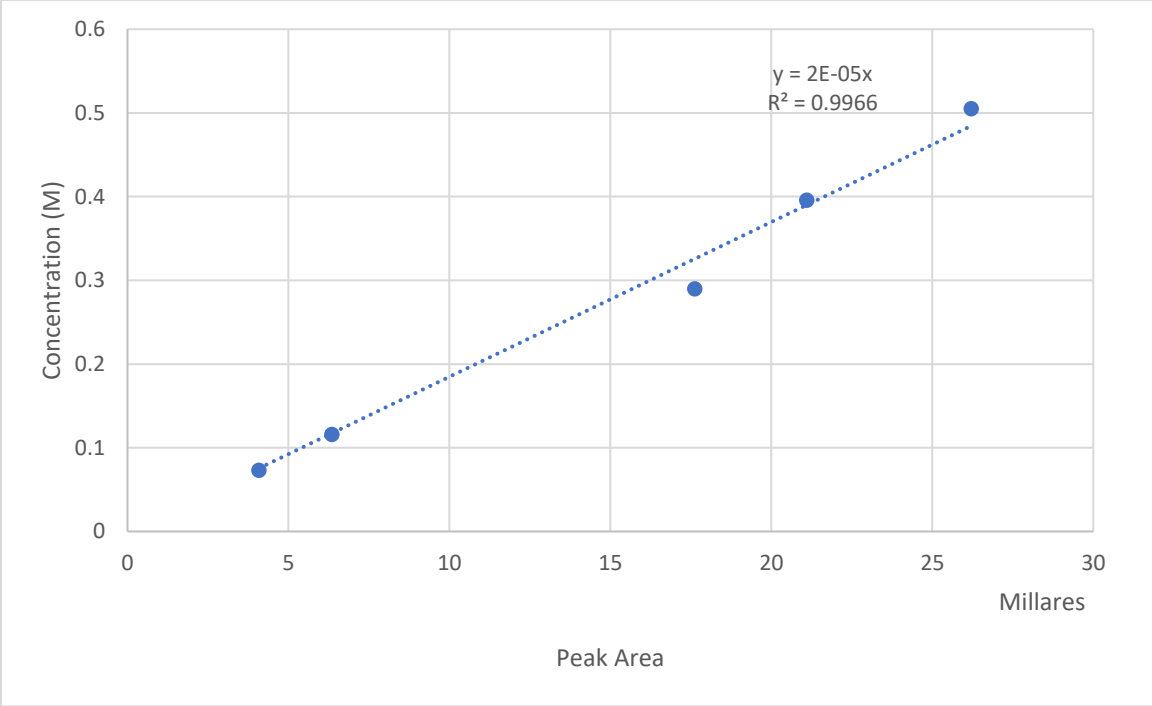

Figure A2. Cyclohexanone calibration curve.

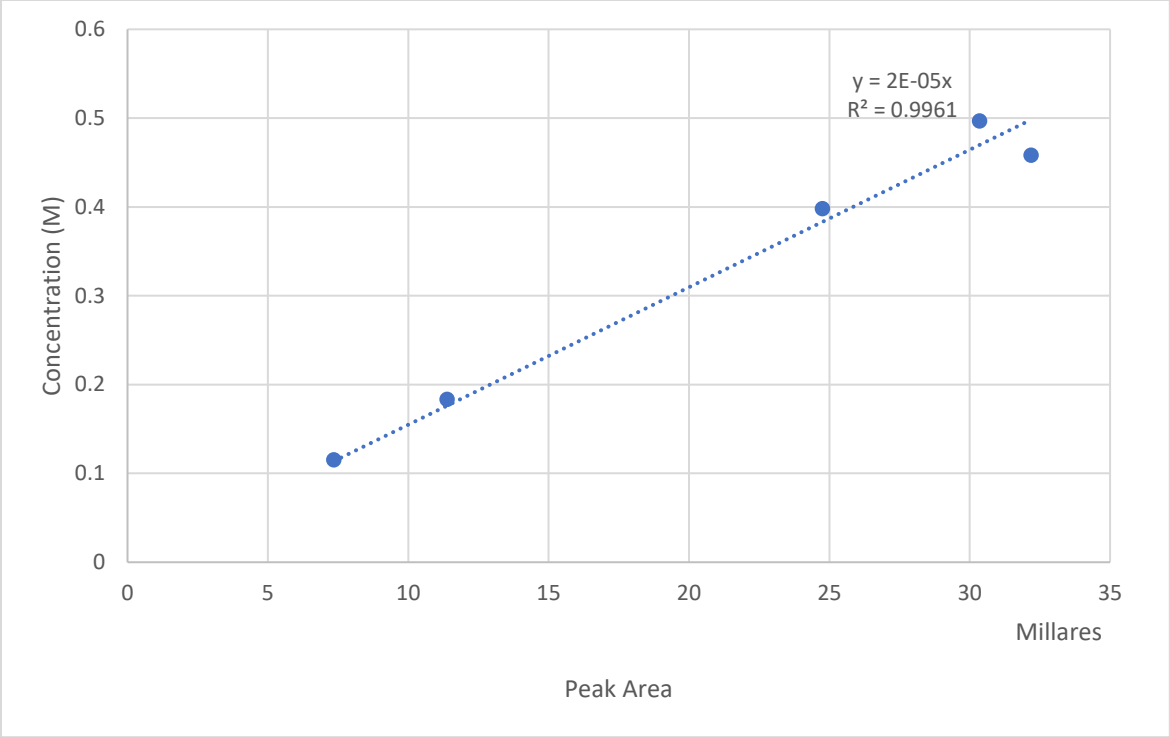

Figure A3. Cyclohexanol calibration curve.

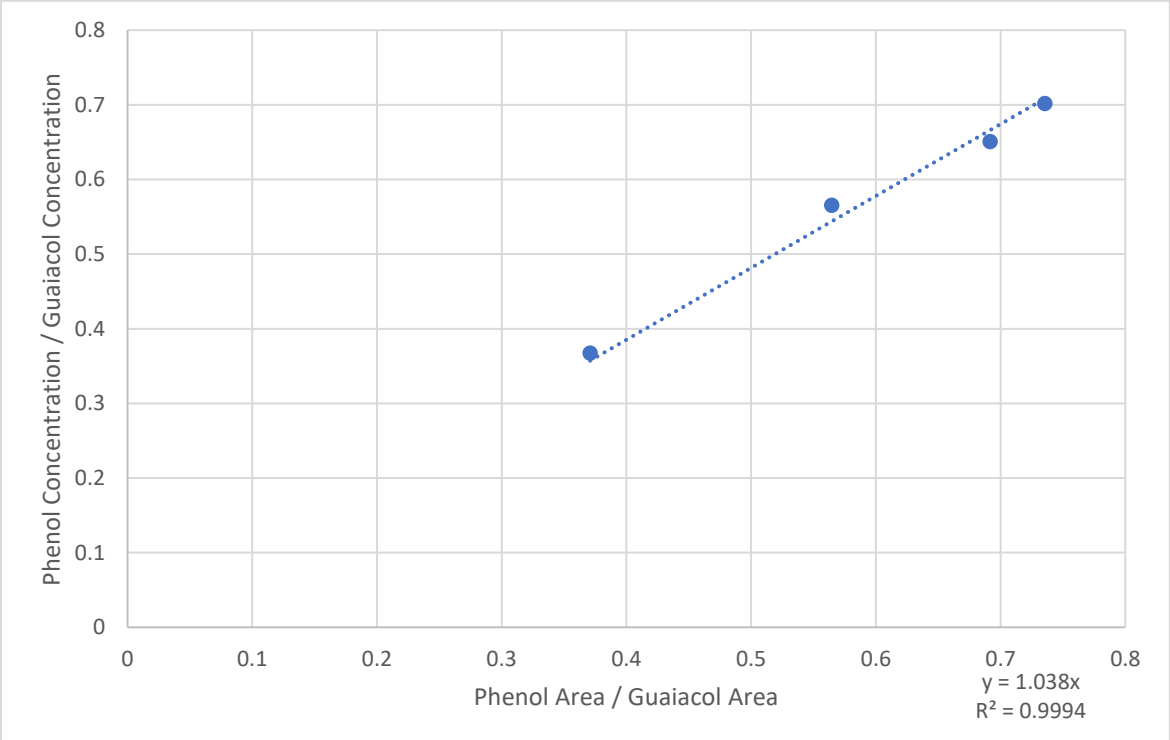

Figure A4. Phenol calibration curve for products in aqueous solution.

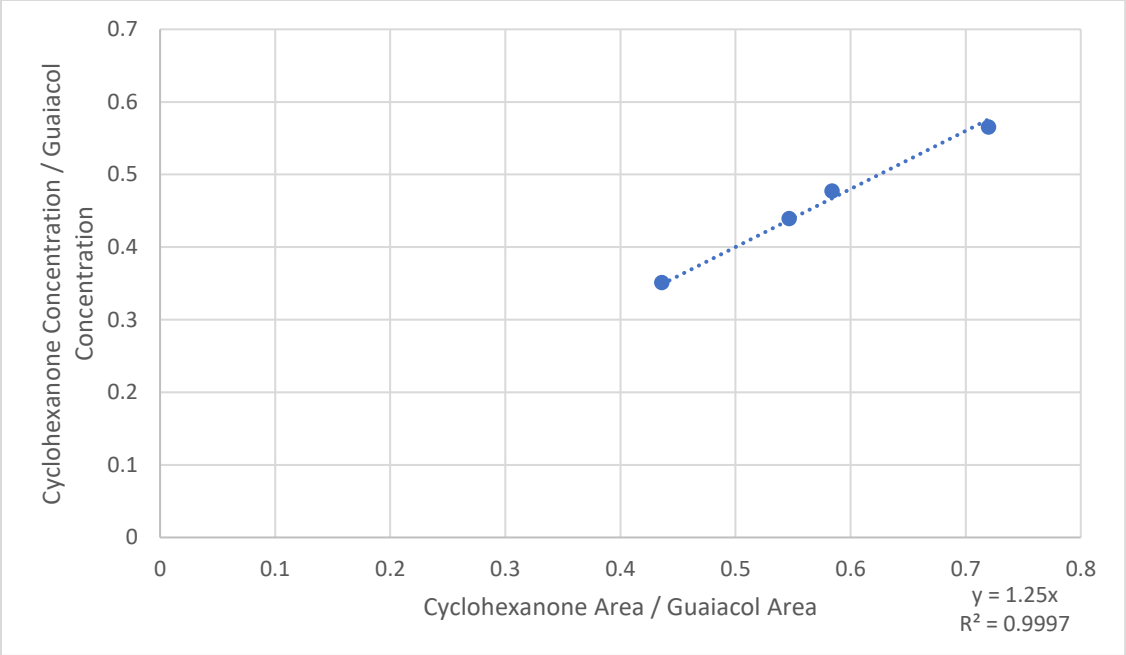

Figure A5. Cyclohexanone calibration curve for products in aqueous solution.

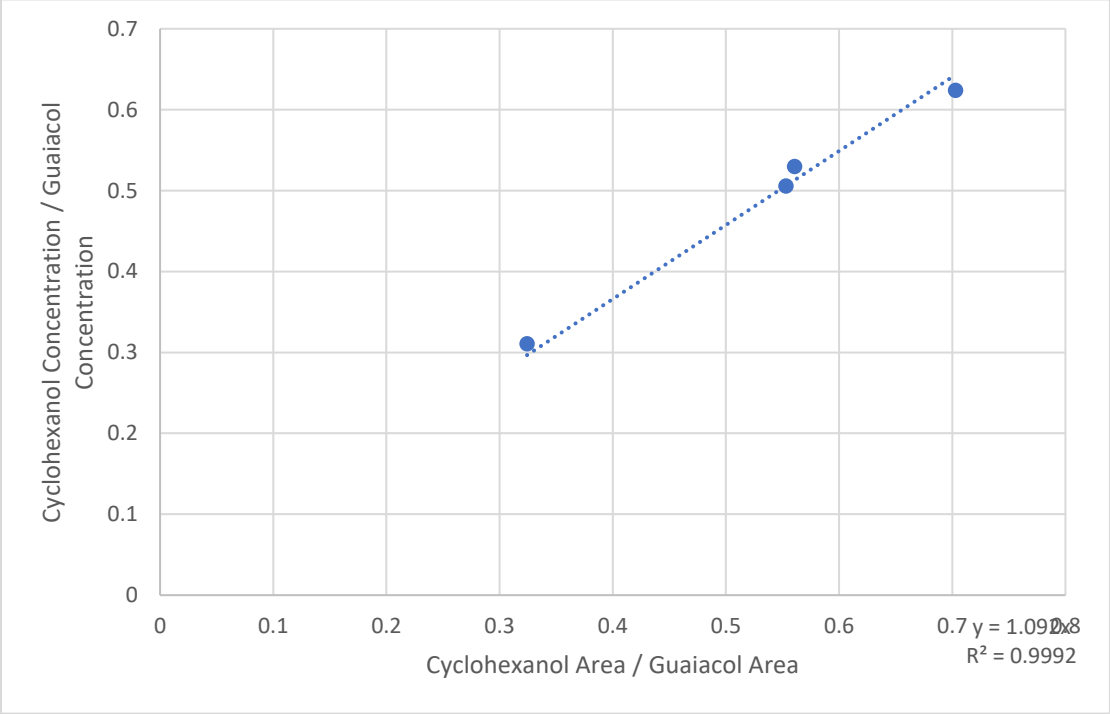

Figure A6. Cyclohexanol calibration curve for products in aqueous solution.

APPENDIX B: WEISZ-PRATER METHOD

The Weisz-Prater number was calculated for each trial that was run to verify that there were no mass and heat transfer limitations so that the kinetic steps were the rate controlling steps in the experimental setup. The procedure for calculating Weisz-Prater criterion was followed as described by M. Albert Vannice[31].

We begin by thinking of the molar flux out from the particle. The rate of reaction *R*, multiplied by the volume *V* of the particle must be equal to the rate of diffusion through the surface of the particle. $AD_{eff}(dC/dr)_{r=Rp}$

$$RV = AD_{eff}\left(\frac{dC}{dr}\right)_{r=R_p}$$

For a spherical particle of radius R_p:

$$R = \frac{3}{R_p} D_{eff}\left(\frac{dC}{dr}\right)_{r=R_p}$$

For mass transfer limitations to be negligible, there must be a negligible concentration gradient over the particle, from the bulk to the center. If this is indeed negligible, the concentration is uniform throughout the particle, meaning diffusion from the particle must be quick. Written explicitly with C_s as the bulk concentration:

$$\left(\frac{dC}{dr}\right)_{r=R_p} \ll \frac{C_s}{R_p}$$

Combining equations:

$$\frac{R_p^2 R}{C_s D_{eff}} \ll 3$$

This can be expanded more precisely so that the criterion on the left-hand side is required to be less than 0.3. The math is not pursued here, as the resulting left-hand side quantity calculated is the same. It is more useful to apply the formula to the experimental system.

All calculations are for values at the initial conditions of reaction. Initial reaction rates are calculated for analysis, and initial concentrations are measured. The radius of the particles was measured using ASME sieves. Diameters of the particles were found to be 45 μm – 63 μm.

Effective diffusivities are more difficult to estimate and will depend on solvent identity. Marten Ternan developed a semi-empirical formula to calculate effective diffusivity with only one fitting parameter in 1987.[44]

$$D_{eff} = D_b \frac{(1-\lambda)^2}{1+P\lambda}$$

Here, λ is a ratio of radius of the diffusing molecule to the radius of the pore, and P is a fitting parameter which can be found empirically for different catalysts. Although a thorough evaluation of P and λ is possible, the uncertainty in bulk diffusivities will be great regardless, and as the final evaluation of the Weisz-Prater number is simply needs to be less than the critical value of 0.3, precise values of P and λ are not strictly necessary.

In his paper, Ternan reviews some examples. One example[45] tests correlation for some light organic solvents and computes a fitting parameter of P = 16.26 that gives remarkable agreement. This P value was used for the calculations in our system.

For lambda, a molecular radius of 0.373 nm and a conservatively large pore radius of 6 nm was used,[46,47] yielding $\lambda = 0.06$.

The bulk diffusivity for each solvent is calculated at reaction conditions (T = 200 °C) using the Wilke-Chang correlation.[48]

The resulting product values ranged from 0.0003 to 0.008 for data used in calculations. One trial did have a Weisz-Prater number of 0.016, which is still much less than 0.3, but much greater than other computed Weisz-Prater numbers. The conversion in this trial was ~70%, leading to a greater reaction rate and thus Weisz-Prater number and disqualifying the results from being used in initial rate calculations.

This test provides quantitative evidence that the experimental setup is free from intraphase gradients.

AUTHOR'S BIOGRAPHY

Daniel McKeon is a chemical engineering major from Searsport, Maine. At the University of Maine, he was a Pulp and Paper Foundation scholar and enrolled in the Honors College. He tutored students in chemistry and worked as a teaching assistant while at UMaine. He held various officer positions in the student chapters of American Institute of Chemical Engineers, Technical Association of the Pulp and Paper Industry, and the engineering honor society, Tau Beta Pi.

Upon graduation, he will be working for the Packaging Corporation of America on process control capital engineering projects.